10.1109/ULTSYM.2014.0317

In vivo Photoacoustic Oxygen Saturation Imaging Without the Need for Fluence Estimation

Erwin J. Alles, Efthymia Papaevangelou and Jeffrey C. Bamber
Joint Department of Physics and CRUK Cancer Imaging Centre at The Institute of Cancer Research
and The Royal Marsden NHS Foundation Trust, London, United Kingdom. Email: Erwin.Alles@ICR.ac.uk

***Abstract*—Due to the difference between the absorption spectra of reduced and oxygenated haemoglobin, spectroscopic photoacoustic imaging can be used to determine, *in vivo* and non-invasively, the local blood oxygen saturation. Conventional methods achieve this by computing the absolute concentrations of reduced and oxygenated haemoglobin, which require models for, or computations of, the local fluence at depth. However, such estimates are potentially inaccurate or expensive to compute.**

In this work, fluence estimation is circumvented by modelling the absorption spectra. Over local wavelength ranges the absorption spectra of reduced and oxygenated haemoglobin can accurately be represented by linear functions, and extrapolating the best-fit straight lines to zero absorption yields a fluence-independent quantity that is readily converted to a blood oxygen saturation level.

Using a clinical photoacoustic scanner, spectroscopic images were obtained from the second author's inner elbow in the wavelength range between 761 and 793 nm. Regions of interest containing signal from either an artery or a vein were analysed with the new method, and yielded oxygen saturation values of 97 % and 70 %, respectively, which are in agreement with literature. Thus, these preliminary results suggest that the presented method can effectively determine local oxygen saturation *in vivo* and at depth.

I. Introduction

In biomedical photoacoustic (PA) imaging, pulsed laser light is shone onto tissue and subsequently absorbed. Upon such absorption the tissue is locally heated, and the resulting thermoelastic expansion generates an acoustic wave that is recorded using conventional ultrasound (US) transducers [1]. Images reconstructed from such recordings exhibit resolutions similar to conventional US images, and penetration depths up to several centimetres. However, as different chromophores have different absorption spectra [2], PA images can show more than just anatomy. Utilising the spectral sensitivity of PA imaging, molecular imaging can be achieved using endogenous contrast molecules such as haemoglobin and melanin, or by administering targeted exogenous contrast agents [3].

Furthermore, the difference between the absorption spectra of reduced (Hb) and oxygenated haemoglobin (HbO) can be exploited to image the local blood oxygen saturation *in vivo* [4], which may be used for predicting or monitoring tumour treatment response. Current oxygen saturation imaging methods attempt to determine the absolute concentrations of Hb and HbO in the blood, from which the oxygen saturation is then computed. However, these methods require either approximate models [4], [5], [6], which are potentially inaccurate, or reconstruction [7], [8], [9] of the local light fluence at depth, which is computationally expensive.

Acknowledgments - The authors wish to thank Zonare Medical Systems Inc., USA, for assistance with equipment and technical support. This research was funded by Cancer Research UK, the Engineering & Physical Sciences Research Council, and the Department of Health.

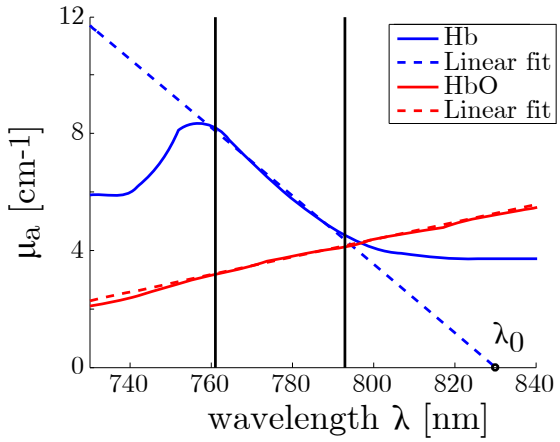

Fig. 1. Absorption spectra of reduced (Hb, blue) and oxygenated haemoglobin (HbO, red) at physiological concentrations. In the wavelength range $761 \leq \lambda \leq 793$ nm (indicated by the black lines) both spectra are approximately linear, and corresponding linear fits over this wavelength range are shown by the dashed lines. Extrapolating such a linear fit to $\mu_a = 0$ yields the zero-crossing wavelength λ_0.

In this work an alternative approach is presented where not the fluence, but the absorption spectrum (and hence the PA spectrum) is modelled. Extrapolating a linear fit of the absorption spectrum yields a fluence-independent quantity from which relative concentrations of Hb and HbO, and hence the blood oxygen saturation, are readily obtained. The remainder of this paper will outline the mathematics and assumptions behind the approach, and show the first preliminary *in vivo* result obtained using this method.

II. Methods

A. Oxygen Saturation Measurement

In Fig. 1 the absorption spectra of reduced and oxygenated haemoglobin, both taken from [10], are shown. Together with melanin these are the dominant endogenous absorbers in the wavelength range accessible by the pulsed wavelength tuneable laser used in this work [11], and hence only these three chromophores will be considered.

As melanin is mainly located in the skin, the effective absorption spectrum of perfused tissue at depth is a linear combination of the absorption spectra of Hb and HbO and hence depends on the blood oxygen saturation. These spectra can, over certain wavelength ranges, accurately be approximated by linear functions, as indicated in Fig. 1 for the wavelength range $761 \leq \lambda \leq 793$ nm.

According to [1], the initial pressure increase $P_0(\vec{r}, \lambda)$ due to light absorption in position $\vec{r}$ at wavelength λ is given by

$$P_0(\vec{r}, \lambda) \;=\; \Gamma(\vec{r}, T)\; \mu_a(\vec{r}, \lambda)\; \phi(\vec{r}, \lambda), \tag{1}$$

where $\Gamma(\vec{r}, T)$ is the Grüneisen coefficient [dimensionless] governing the conversion from optical to acoustical energy, $\mu_a(\vec{r}, \lambda)$ is the effective absorption coefficient [cm^{-1}], $\phi(\vec{r}, \lambda)$ is the local light fluence [J/cm^2], and T is the temperature [°C].

Under the assumptions

$$\begin{aligned} \mu_a(\vec{r}, \lambda) &\approx c(\vec{r})\,[\gamma(\vec{r})\lambda + \delta(\vec{r})]\,, \\ \phi(\vec{r}, \lambda) &\approx \phi(\vec{r}), \end{aligned} \tag{2}$$

where $c(\vec{r})$ is the local haemoglobin concentration (of both Hb and HbO) [mol], $[\gamma(\vec{r})\lambda + \delta(\vec{r})]$ is the linearised effective normalised absorption spectrum, and fluence $\phi(\vec{r})$ is wavelength-independent, equation (1) reduces to

$$P_0(\vec{r}, \lambda) \approx \Gamma(\vec{r}, T)\; \phi(\vec{r})\; c(\vec{r})\,[\gamma(\vec{r})\lambda + \delta(\vec{r})]\,. \tag{3}$$

Setting $P_0(\vec{r}, \lambda) = 0$ gives

$$\Gamma(\vec{r}, T)\; \phi(\vec{r})\; c(\vec{r}) = 0, \tag{4}$$

a situation where no PA signal would be generated regardless of the wavelength as either the fluence, the haemoglobin concentration or the Grüneisen coefficient equals zero, or

$$[\gamma(\vec{r})\lambda + \delta(\vec{r})] = 0 \;\Rightarrow\; \lambda_0 = -\frac{\delta(\vec{r})}{\gamma(\vec{r})}, \tag{5}$$

which gives the wavelength λ_0 at which the linearised effective absorption coefficient equals zero (see Fig. 1). While this wavelength has no physical meaning, as at an absorption coefficient of zero no PA signal would be generated, it does form a fluence-independent parameter that can be used to characterise the actual absorption spectrum within an approximately linear region.

Within this linear region, the absorption spectra of HbO and Hb are approximated by

$$\begin{aligned} \mu_{\mathrm{a,HbO}}(\vec{r}, \lambda) &\approx c(\vec{r})\,[\gamma_{\mathrm{HbO}}\lambda + \delta_{\mathrm{HbO}}]\,, \\ \mu_{\mathrm{a,Hb}}(\vec{r}, \lambda) &\approx c(\vec{r})\,[\gamma_{\mathrm{Hb}}\lambda + \delta_{\mathrm{Hb}}]\,, \end{aligned} \tag{6}$$

respectively, where γ and δ are the slopes and zero-offsets of the linear fits, respectively. For a given oxygen saturation $z = c_{\mathrm{HbO}}(\vec{r})/(c_{\mathrm{Hb}}(\vec{r}) + c_{\mathrm{HbO}}(\vec{r}))$, with c_{Hb} and c_{HbO} denoting the absolute concentrations of Hb and HbO, respectively, the effective absorption coefficient $\mu_{\mathrm{a,eff}}$ can thus be approximated by

$$\begin{aligned} \mu_{\mathrm{a,eff}}(\vec{r}, \lambda, z) = c(\vec{r})[&\quad \{z\,\gamma_{\mathrm{HbO}} + (1-z)\gamma_{\mathrm{Hb}}\}\,\lambda \\ &+ \{z\,\delta_{\mathrm{HbO}} + (1-z)\delta_{\mathrm{Hb}}\}]. \end{aligned} \tag{7}$$

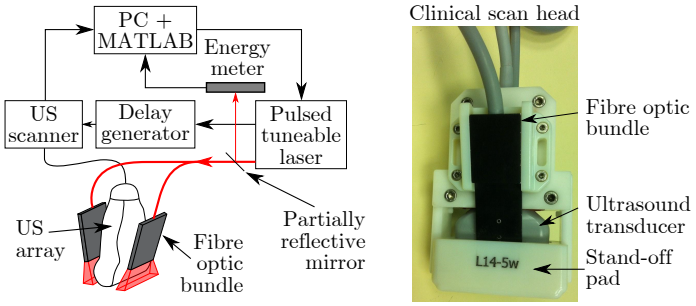

Fig. 2. Schematic (left) of the hardware of the fully automated spectroscopic epiphotoacoustic scanner, and photograph (right) of the clinical scan-head.

Setting equation (7) to zero yields the zero-crossing wavelength λ_0, which can in turn be solved for z to yield

$$z = \frac{\lambda_0 - \lambda_{0,\mathrm{Hb}}}{\lambda_0 - \lambda_{0,\mathrm{Hb}} - \frac{\gamma_{\mathrm{HbO}}}{\gamma_{\mathrm{Hb}}}(\lambda_0 - \lambda_{0,\mathrm{HbO}})}, \tag{8}$$

where the constants

$$\lambda_{0,\mathrm{HbO}} = -\frac{\delta_{\mathrm{HbO}}}{\gamma_{\mathrm{HbO}}},\; \lambda_{0,\mathrm{Hb}} = -\frac{\delta_{\mathrm{Hb}}}{\gamma_{\mathrm{Hb}}},\; \text{and}\; \frac{\gamma_{\mathrm{HbO}}}{\gamma_{\mathrm{Hb}}} \tag{9}$$

can be obtained experimentally using reference blood samples, or from literature. Thus, by performing spectroscopic PA measurements over a wavelength range in which the absorption spectra of both Hb and HbO are approximately linear, the slope and offset of the resulting PA spectrum are readily translated into an oxygen saturation z using equation (8).

B. Clinical Spectroscopic PA Imaging System

Spectroscopic PA data were acquired *in vivo* using an in-house developed clinical system consisting of a tuneable pulsed laser (Quantel Brilliant B + Rainbow OPO, $685 \leq \lambda \leq 950$ nm) connected to a clinical ultrasound scanner (Zonare Ultra + Z.one® research package 4.7) using a linear transducer array with a centre frequency of 12 MHz and a bandwidth of 42% (Zonare L14-5w). Part of the laser beam was reflected using a partially reflective mirror (Thorlabs CM1BP108) onto a pulse energy monitor (Gentec EO S-LINK-2 + QE12LP-SMB) to yield the pulse-by-pulse energy measurements used to correct the PA spectra for laser pulse energy variations, while the remainder of the beam was transported to the scan-head using a bifurcated fibre-optic bundle. All devices were controlled in a fully automated fashion by a PC running MATLAB R2013A, as shown in the system sketch on the left in Fig. 2.

The ultrasound transducer and fibre-optic bundles were mounted in the 3D-printed scan-head assembly shown on the right in Fig. 2, the geometry of which was based on the results reported in [12]. A stand-off pad of 20 mm height, consisting of 10 %-mass gelatine in water, was added to temporally separate the PA signal generated in the tissue from the pulse echo signal generated by the photoacoustic effect at the transducer surface [13], [14].

PA images, which are coregistered with conventional ultrasound images, were acquired using single laser pulses, and reconstructed off-line using the k-space Fourier reconstruction

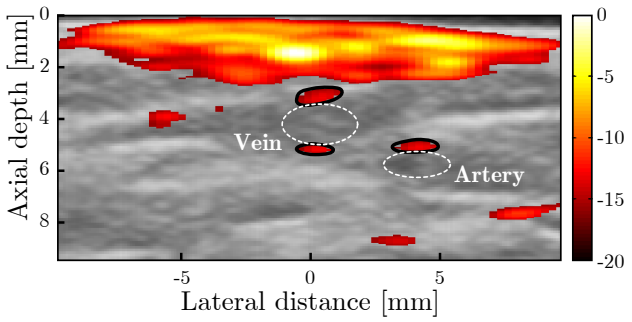

Fig. 3. Photoacoustic (PA) image of the second author's inner elbow overlaid on a gray-scale B-mode image. The image is displayed on a normalised logarithmic scale with a dynamic range of 20 dB. The approximate locations of an artery and a vein (confirmed using colour Doppler in unreported experiments) are indicated by white ellipses, and the corresponding regions of interest used to measure the PA spectra are shown by the solid black outlines.

method [15]. Only the centre 64 elements of this transducer were used and data was exported using a sampling frequency of 30 MHz. As is visible in Fig. 1, the wavelength region with the strongest difference in slope between linear fits of the absorption spectra of Hb and HbO is the region $761 \leq \lambda \leq 793$ nm, which was therefore used in this work. This wavelength range was scanned at 4 nm intervals to yield nine PA images which were subsequently analysed by computing the average PA amplitude within a region of interest.

III. Results

To test the method, spectroscopic PA images were taken of the second author's inner elbow. One such image, acquired using a wavelength of 761 nm, is shown in Fig. 3 together with the corresponding B-mode image. The locations of an artery and a vein (verified using colour Doppler) are indicated. Signal from the skin, the artery, and the vein can clearly be identified, and additional signal of unknown origin can be observed. Due to the limited acoustic bandwidth and aperture, the chosen image reconstruction algorithm recovers only the top and bottom of the blood vessels.

The PA spectra of the artery and vein were obtained by averaging the PA amplitude inside the regions of interest indicated in Fig. 3, and are plotted in Fig. 4 (solid lines). Linear fits of the measured data are plotted using dashed lines, and the absorption spectra of Hb and HbO and their linear fits are shown for comparison. Note that the highly oxygenated arterial blood produces a PA spectrum that closely resembles that of HbO, whereas the PA spectrum of venous blood is a mixture of that of Hb and HbO.

Extrapolating the linear fits to the PA spectra yields the zero-crossing wavelength $\lambda_0 = 630$ nm for the artery, whereas for the vein $\lambda_0 = 1166$ nm. Using equation (8) and taking the reference absorption spectra of Hb and HbO from [10], these zero-crossings yield the oxygen saturations $z_{\text{artery}} = 97$ % and $z_{\text{vein}} = 70$ %. These values agree with literature values for oxygen saturation levels in both arterial ($93.5 - 97.5$ %) and venous blood ($55.3 - 70.7$ %) [16, p.169].

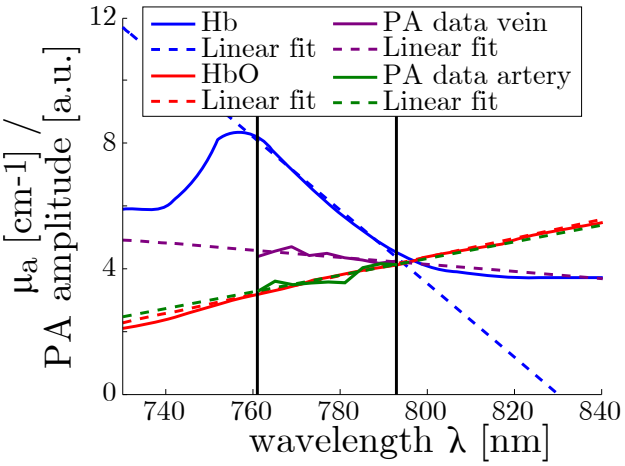

Fig. 4. Photoacoustic spectra obtained from signal originating from a vein (purple solid line) and an artery (green solid line) together with the reference absorption spectra of reduced (blue solid line) and oxygenated haemoglobin (red solid line). Corresponding linear fits to the data in the wavelength range $761 \leq \lambda \leq 794$ nm are shown using dashed lines. PA spectra are scaled to ensure all four linear fits cross at the same wavelength of $\lambda \approx 795$ nm.

IV. Discussion and Conclusion

By modelling the chromophore absorption spectra and computing relative rather than absolute Hb and HbO concentrations, the need for an accurate model, or estimate, of the local fluence is eliminated, which reduces computational cost and potentially reduces inaccuracies. While the results presented above are encouraging, their accuracy needs to be confirmed by comparing with simultaneously acquired direct oxygen saturation measurements. To this aim, both phantom and *in vivo* experiments are planned.

Inaccuracies may arise from the limited validity of the assumptions underlying the method. In this work, absorption is limited to only Hb and HbO, and the local fluence is assumed to be wavelength-independent over the studied wavelength range. In reality, absorption by melanin in the skin, scattering within the tissue and strong absorption will result in a wavelength-dependence in the fluence that increases with depth.

The absorption by melanin should be compensated for by calibration. This requires measurement of the absolute concentration of melanin in the skin, which could be derived from, e.g., colorimetric or spectroscopic PA measurements of the skin.

The wavelength-dependence due to scattering can be reduced by choosing a narrow wavelength range, although this might reduce the sensitivity of the method, or by selecting an optimal wavelength range. In this work the wavelength range was chosen that maximised the PA amplitude and spectral difference between Hb and HbO, but a different choice might result in improved accuracy.

The influence of strong local absorption on the spectrum of the light at depth is likely to be weak as the multiple scattering observed in biomedical tissue can deliver light to locations below a localised absorber. However, non-localised absorption

occurring in, for example, dense tumour vasculature is likely to have a significant impact on the fluence spectrum and could limit the accuracy of the method at depth.

By performing linear fitting to spectroscopic PA data, the influence of noise and laser pulse energy measurement errors on the oxygen saturation measurement is greatly reduced. However, the presence of noise will bias the obtained saturation value by increasing the zero-offset δ in equation (5), especially in regions of low signal amplitude. Therefore, rather than using literature values for the constants in equation (9), the method needs to be calibrated against other techniques both *in vivo* and using reference blood samples.

The results presented here were obtained with an in-house developed spectroscopic PA scanner that required around 3 s to tune between wavelengths, resulting in a total acquisition time of around 30 s. As the scan-head assembly was hand-held during acquisition, this resulted in motion artifacts in the PA images which prohibited high-resolution imaging of the blood oxygen saturation. To suppress these motion artifacts, large regions of interest were analysed. To avoid the resulting loss of spatial resolution, these motion artifacts can be reduced by applying motion compensation schemes or increasing the frame-rate of the PA scanner.

In conclusion, the method presented here measured, *in vivo* and non-invasively, the local blood oxygen saturation state and yielded, for the case studied, values that agreed with published work. While the method is not exact and requires further optimisation, calibration and evaluation, it shows great promise as an easily implemented, real-time imaging method.

REFERENCES

[1] P. Beard, "Biomedical photoacoustic imaging," *Interface Focus*, vol. 1, no. 4, pp. 602–631, 2011.

[2] S. L. Jacques, "Optical properties of biological tissues: a review," *Phys Med Biol*, vol. 58, no. 11, pp. R37–R61, 2013.

[3] C. Kim, E. C. Cho, J. Chen, K. H. Song, L. Au, C. Favazza, Q. Zhang, C. M. Cobley, F. Gao, and Y. Xia, "In vivo molecular photoacoustic tomography of melanomas targeted by bioconjugated gold nanocages," *ACS nano*, vol. 4, no. 8, pp. 4559–4564, 2010.

[4] X. Wang, X. Xie, G. Ku, L. V. Wang, and G. Stoica, "Noninvasive imaging of hemoglobin concentration and oxygenation in the rat brain using high-resolution photoacoustic tomography," *J Biomed Optic*, vol. 11, no. 2, pp. 024 015/1 – 024 015/9, 2006.

[5] S. Kim, Y.-S. Chen, G. P. Luke, and S. Y. Emelianov, "In vivo three-dimensional spectroscopic photoacoustic imaging for monitoring nanoparticle delivery," *Biomed Opt Express*, vol. 2, no. 9, pp. 2540–2550, 2011.

[6] D. Razansky, A. Buehler, and V. Ntziachristos, "Volumetric real-time multispectral optoacoustic tomography of biomarkers," *Nat Protoc*, vol. 6, no. 8, pp. 1121–1129, 2011.

[7] B. T. Cox, S. R. Arridge, K. P. Kstli, and P. C. Beard, "Two-dimensional quantitative photoacoustic image reconstruction of absorption distributions in scattering media by use of a simple iterative method," *Appl Opt*, vol. 45, no. 8, pp. 1866–1875, 2006.

[8] J. Laufer, E. Zhang, and P. Beard, "Quantitative in-vivo measurements of blood oxygen saturation using multiwavelength photoacoustic imaging," in *proc of BiOS*, 2007, pp. 64 371Z1–64 371Z9.

[9] T. Jetzfellner, D. Razansky, A. Rosenthal, R. Schulz, K.-H. Englmeier, and V. Ntziachristos, "Performance of iterative optoacoustic tomography with experimental data," *Appl Phys Lett*, vol. 95, no. 1, p. 013703, 2009.

[10] S. Prahl, *Optical Absorption of Hemoglobin*. omlc.ogi.edu/spectra/hemoglobin/: , 1999, accessed on 14 June 2014.

[11] J. Moan, *Ch 7 of Visible Light and UV Radiation*. Oslo, Norway: Scandinavian Science Publisher, 2001, pp. 69–85.

[12] E. J. Alles, D. Harris-Birtill, M. Jaeger, and J. C. Bamber, "Performance characterisation of a new clinical spectroscopic epiphotoacoustic scanner," in *proc of IEEE IUS*, 2013, pp. 1845–1848.

[13] M. Jaeger, D. Birtill, A. Gertsch, E. OFlynn, and J. Bamber, "Clinical feasibility of duplex photoacoustic and ultrasound pulse-echo imaging using photoacoustic transmit pulses," in *proc of IEEE IUS*, 2011.

[14] M. Jaeger, D. Harris-Birtill, A. Gertsch, E. OFlynn, and J. Bamber, "Deformation-compensated averaging for clutter reduction in epiphotoacoustic imaging in vivo," *J Biomed Optic*, vol. 17, no. 6, pp. 0 660 071–0 660 078, 2012.

[15] M. Jaeger, S. Schüpbach, A. Gertsch, M. Kitz, and M. Frenz, "Fourier reconstruction in optoacoustic imaging using truncated regularized inverse k-space interpolation," *Inverse Probl*, vol. 23, pp. S51–S63, 2007.

[16] P. L. Altman and D. D. Katz, *Blood and Other Body Fluids*. Madison, WI: Federation of American Societies for Experimental Biology, 1961.